A 30-year ocean front dataset from 1993 to 2023 for the Northwest Pacific Ocean based on deep learning ~~from 1993 to 2023 for Northwest Pacific ocean~~

Yuan Niu[1], Xuefeng Zhang[1], Dianjun Zhang[1]

[1]School of Marine Science and Technology, Tianjin University, Tianjin 300072, China

Correspondence to: Dianjun Zhang (zhangdianjun@tju.edu.cn)

Abstract. Ocean fronts are critical interfaces between different water masses and~~,~~ profoundly influence atmosphere–ocean interactions, weather systems, marine ecosystems, and climate regulation. Accurate and long-term observations of ocean fronts are essential for advancing studies in meteorology, oceanography, and climate science. However, no publicly available, long-term ocean front dataset currently exists, and the existing detection methods often rely on time-consuming manual labelling or traditional algorithms with limited accuracy in complex frontal regions. In this study, we release the first publicly available 30-year ocean front dataset (1993–2023) for the Northwest Pacific, which was generated by applying a deep learning framework (Mask R-CNN) to daily sea surface temperature (SST) fields, with manually annotated samples for model training. The dataset provides pixel-level frontal boundaries along with the associated attributes, including the position, intensity, and width, stored in NetCDF-4 format at a 1/12° spatial and daily temporal resolution. An a~~A~~ccuracy evaluation shows that the~~a~~ mean average precision (mAP) ~~exceeding~~ exceeds 0.90, and compared with traditional gradient methods, the errors in front width and intensity are smaller~~with smaller errors in front width and intensity compared with traditional gradient-based methods, while capturing more small-scale features~~. The dataset offers three main contributions: (1) It fills a~~Filling the~~ critical gap by providing~~of~~ a standardized, long-term ocean front product; (2) it serves~~Serving~~ as a ready-to-use training resource for deep learning models~~,~~ that greatly ~~reducing~~ reduces the need for manual labelling; and (3) it provides~~Providing~~ benchmark samples for validation and intercomparison of other ocean front detection products. This dataset supports robust investigations of the seasonal-to-interannual frontal variability and provides a valuable foundation for applications in meteorology, ecosystem management and climate change research.

1 Introduction

An ocean front refers to a narrow transition zone between two or more water masses with significantly different properties, where oceanographic parameters such as the temperature, salinity, and water colour experience sharp changes. It can be characterized by the horizontal gradient of the sea surface temperature (Chen, 2009; Wang and Wang, 2015). As an important intersection between the atmosphere and the ocean, the ocean front holds a significant position in the field of Earth science (Lachkar et al., 2011; Azevedo et al., 2021). ~~Ocean front refers to a narrow transitional zone between two or more types of water bodies with significantly different properties, which is a jumping zone of marine environmental parameters and can be described by the horizontal gradient of seawater temperature. As an important intersection between the atmosphere and the~~

ocean, ocean front holds a significant position in the field of Earth science . These fronts are the places where different air masses (usually cold and warm humid air) interact, not only having profound impacts on meteorology and climate, but also playing key roles in ecology, resource management, and climate regulation . From extreme weather events to changes in marine ecosystems, to the stability of the global climate system, ocean fronts are important in multiple fieldsthe importance of ocean fronts cannot be ignored in multiple fields (Belkin et al., 2009). Ocean front recognition is of crucial importance for meteorological and climate research, and ocean front detection is crucial for meteorological and climate research (Chronis, 2021). By accurately identifying and tracking ocean fronts, it is possible to better understand the dynamics of climate and weather systems, thereby providing early warning for extreme weather events (Saldías et al., 2021). The identification of ocean fronts can help us better understand the Earth's climate and ecosystem, providing support for global climate change research (Ruiz, 2019).

The data sources for ocean front extraction include SeaWiFS water colour data (Belkin and O'reilly, 2009), MODIS sea surface temperature (SST), and AVHRR SST remote sensing image data (Shaw and Vennell, 2001). At present, the main methods for extracting ocean fronts based on remote sensing data include statistical histogram method , gradient method , Canny algorithm , wavelet analysis , the mathematical morphology method , the entropy theory algorithm and gravity model based methods . The main methods for front detection are population-based(Cayula and Cornillon, 1992; Nieto et al., 2012; Roa-Pascuali et al., 2015; Diehl et al., 2002) and gradient-based(Oram et al., 2008; Davis, 1975). Cayula and Cornillon proposed the single-image edge detection (SIED) algorithm based on histogram analysis. This algorithm demonstrates effective detection performance and has been widely applied in ocean front detection. The gradient algorithm is a commonly used ocean front detection method and includes the Sobel operator, Prewitt operator, Laplacian operator, and other gradient operators. The main methods for calculating temperature gradients are Gradient method and Sobel gradient algorithm. However, these algorithms may not effectively distinguish between genuine ocean fronts and other image features or artifacts. They can produce false positives or miss actual fronts, compromising the accuracy and reliability of the detection results. Traditional methods often lack the adaptability to handle varying oceanographic conditions and environmental factors. They may struggle to detect ocean fronts in regions with weak or ambiguous front edges, where the information is less pronounced and subject to fluctuations. This limitation restricts their application in dynamically changing marine environments. Since 1970s, significant progress has been made in the detection and research for ocean fronts. The gradient algorithm is a commonly used ocean front detection method, such as the Sobel operator, Prewitt operator, Laplacian operator, and other gradient operators (Davis, 1975). However, these operators are too sensitive to noise and have poor performance in detecting small edges. Ping et al. (2014) proposed an ocean front detection method based on threshold intervals and Bayesian decision theory. This method uses the Sobel operator to compute the gradient map of SST images and determines the threshold interval by using a gradient histogram, ultimately achieving ocean front detection (Ping et al., 2014). Traditional gradient threshold methods rely on setting a threshold value to identify sea fronts manually (Fan et al., 2009). However, the selection of this threshold is subjective and lacks a standardized criterion. In addition, different researchers or studies may choose different threshold values, leading to inconsistency and variability in the detected ocean fronts.Ping et al. (2014) proposed a dual-I value ocean front recognition method based on the gradient-I value method. The Sobel operator was used to calculate the gradient map of the SST image, and the dual-I value interval was determined using the gradient histogram method, ultimately completing the recognition of the ocean front . Traditional gradient threshold methods rely on setting a threshold value to identify sea fronts manually . However, the selection of this threshold is subjective and lacks a standardized criterion. Different researchers or studies may choose different threshold values, leading to inconsistency and variability in the detected ocean fronts. Traditional methods based on gradient thresholds often struggle to accurately detect complex and diverse ocean fronts. These methods may overlook subtle variations in the gradient values or fail to capture the intricate patterns and transitions associated with complex fronts. This limitation hampers the ability to comprehensively study and understand the dynamics of ocean fronts. In summary, traditional methods for extracting ocean fronts suffer from limitations such as subjective threshold selection, inadequate handling of complex fronts, dependency on edge detection algorithms, and limited adaptability to changing conditions. Overcoming these limitations is essential for achieving accurate and comprehensive detection of ocean fronts.

With the continuous deepening of deep learning research, convolutional neural networks (CNNs) and R-CNNs have achieved great success in various scenarios, such as image recognitiondetection, speech recognitiondetection, and mouth target

~~recognition~~detection ~~-~~(Yang et al., 2018; Chen et al., 2020; Markus et al., 2019). On this basis, the Mask R-CNN network achieved pixel~~-~~-level instance segmentation of images (He et al., 2017). Lima et al. (2017) proposed a fine-tuning neural network for ocean front detection based on previous research to address ~~the~~ practical situations ~~where~~ in which deep networks such as AlexNet, Caffe Net, GoogLeNet, and VGGNet are prone to overfitting under limited training data. Sun et al. (2019) proposed a multi~~-~~scale detection framework for ocean front detection and fine-grained positions, and Li et al. (2019) proposed an ocean front ~~recognition~~detection network based on the CNN to address the weak edges of ocean fronts. ~~In order t~~To detect more precise ocean fronts, the network fuse~~s~~d the convolutional features at each stage and use~~s~~d the Intersection over Union (IoU)~~the IOU~~ loss function and binary cross~~-~~-entropy loss function to fix model ~~mistakes~~errors. Xie et al (2021) used LSENet to detect and locate multiple ocean fronts in colour SST gradient maps, achieving an ocean front ~~recognition~~detection breakthrough with an mean Dice Similarity Coefficient (mDSC) ~~mDSC~~ greater~~higher~~ than 90%~~-~~, and~~.~~ Li et al. proposed a deep learning model with a U-Net architecture that ~~was~~ is designed to detect and locate significant frontal zones in grayscale sea surface temperature images and successively developed a bidirectional edge detection network (BEDNet)(Li et al., 2020) and weak edge identification network (WEIN) (Li et al., 2022). Niu et al. designed a multi-scale ~~model s~~Simple and qQuick network~~Net~~ (SQNet) model to identify the positions of ocean fronts based on their characteristics~~for identifying the position of ocean fronts based on their characteristics~~ (Niu et al., 2023), and~~.~~ Felt et al. proposed machine learning (ML) models to detect temperature and chlorophyll ocean fronts from unprocessed and radiometrically uncorrected satellite imagery via~~by~~ transfer learning from ~~the~~ existing models for edge detection (Felt et al., 2023).

Table 1. Overview of the existing classic research on ocean front extraction based on deep learning approaches

Author	Experimental area	Network model	Result accuracy	Advantages	Limitations
Lima et al. (2017)	Small regions	CNN	88%	Method involves CNNs and transfer learning via finetuning	Low image resolution
Sun et al. (2019)	Small regions	AlexNet	90%	Six scanning scales	The experimental area is too small
Li et al. (2022)	30-34°N, 132-140°E	U-Net	90%	Small time cost	The ~~recognition~~detection effect of complex sea areas needs to be verified
Niu et al. (2023)	The coast of China and the Gulf of Mexico	SQNet	90%	Based on a multi-scale	The research area is small
Felt et al (2023)	Coastal regions	CNN	90%	Improved computational efficiency	Too few samples in the dataset

With the application of de~~epth~~ learning in the field of image ~~recognition~~detection (Nogueira et al., 2016), and in view of the shortcomings of traditional gradient threshold~~ocean front detection~~ methods, ~~the~~ ocean front detection algorithms based on de~~epth~~ learning ha~~ve~~s become a research hotspot. Sufficient training samples are the basis of target detection based on deep learning. The fusion of ocean front detection and deep learning can yield sufficient~~build enough~~ training data with high integration cost and scarce data, ~~especially in the weak ocean front area where the information of ocean front edge is changeable and not obvious,~~ which increases the difficulty of data set construction. Therefore, considering the small amount of data and the lack of standardized criteria in traditional methods, this paper proposes a new automatic ocean front detection method that applies~~Therefore, considering the small amount of data and weak edge of ocean front, this paper proposed a new automatic detection method of ocean front, which applies~~ Mask R-CNN ~~network~~ to ocean front detection~~,~~ and then achieves~~realizes~~ high-

precision detection of the ocean front ~~through~~ via multiple iterative training steps and parameter correction.

2 Study area and data

~~2.1 Study area~~

The study area for this research ~~is spanning~~spans a latitudinal~~e~~ range of 0° to 50°N and a longitudinal~~e~~ range of 100° to 150°E (Fig.1). The worldwide ocean eddy-resolving (1/12° horizontal resolution, 50 vertical levels) reanalysis encompassing the altimetry (1993 forward) was~~is~~ provided by the Copernicus Marine Environment Monitoring Service (CMEMS) and is available as the GLORYS12V1 product. It is based largely on the current real-time global forecasting CMEMS system. The model component~~s~~ include~~is~~ the Nucleus for European Modelling of the Ocean (NEMO) platform driven at the surface by the European Centre for Medium-Range Weather Forecasts (ECMWF) ERA-Interim ~~then~~and the ERA5 reanalyses for recent years. Observations are assimilated by means of a reduced-order Kalman filter. The sea surface temperature, sea ice concentration, in situ temperature and salinity vertical profiles are jointly assimilated along the track altimeter data.~~Along track altimeter data, Sea Surface Temperature, Sea Ice Concentration and in-situ Temperature and Salinity vertical Profiles are jointly assimilated.~~ Moreover, a 3D-VAR scheme provides a correction for the slowly -evolving large-scale biases in temperature and salinity. This product includes daily and monthly mean files for the temperature, salinity, currents, sea level, mixed layer depth and ice parameters ~~from the top to the bottom.~~ The global ocean output files are ~~display~~provided on a standard regular grid at 1/12° (approximately 9 km) and 50 standard levels. The data used in this work were sourced from~~article is~~ the daily average sea surface temperature dataset, covering a period of 30 years from 1993 to 2023. The units are °C; the temporal resolution is daily; and the spatial resolution is 1/12°.~~The unit is Celsius, the time resolution is day, and the spatial resolution is 1/12°.~~ The specific parameter information for~~of~~ the data is shown in Table 2 (https://data.marine.copernicus.eu/product/).

~~The research area includes Bohai Sea, Yellow Sea, East China Sea, South China Sea, and Western Pacific. These waters cover various ecosystems such as coastal plains, deep trenches, islands, and coral reefs. The marine hydrological conditions are diverse, covering temperate, subtropical, and tropical waters. The changes in ocean temperature, salinity, and ocean currents have significant impacts on marine ecology and climate. The convergence of ocean currents such as the East China Sea Warm Current, Kuroshio, and Philippine Current in this region has a significant impact on marine ecology and climate change. And it has abundant marine resources, including fishery resources, oil and natural gas reserves, mineral resources, as well as renewable energy such as wind and tidal energy. By specifically examining this region, the research aims to gain insights into the dynamics of ocean fronts and their characteristics in this area. Understanding the behavior and distribution of ocean fronts in the South China Sea is crucial for various applications, including marine ecology, fisheries management, and weather prediction. The chosen geographic extent provides a representative and comprehensive view of the oceanic features and processes occurring in this dynamic and economically important region.~~

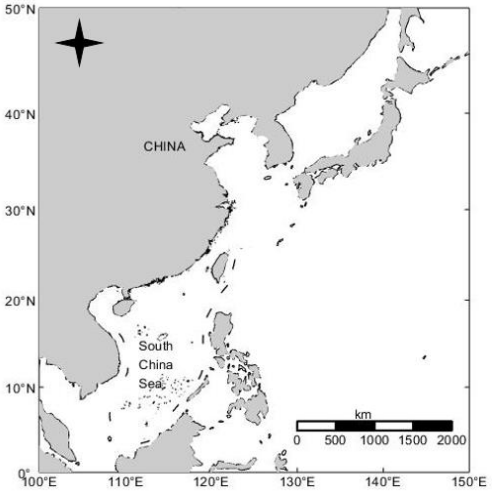

Figure 1. Location of the study area

~~**2.2 Data sources**~~

~~The worldwide ocean eddy-resolving (1/12° horizontal resolution, 50 vertical levels) reanalysis encompassing the altimetry (1993 forward) is provided by the Copernicus Marine Environment Monitoring Service (CMEMS) and is available as the GLORYS12V1 product. It is based largely on the current real-time global forecasting CMEMS system. The model component is the Nucleus for European Modelling of the Ocean (NEMO) platform driven at surface by European Centre for Medium-Range Weather Forecasts (ECMWF) ERA-Interim then ERA5 reanalyses for recent years. Observations are assimilated by means of a reduced-order Kalman filter. Along track altimeter data, Sea Surface Temperature, Sea Ice Concentration and in-situ Temperature and Salinity vertical Profiles are jointly assimilated. Moreover, a 3D-VAR scheme provides a correction for the slowly evolving large-scale biases in temperature and salinity. This product includes daily and monthly mean files for temperature, salinity, currents, sea level, mixed layer depth and ice parameters from the top to the bottom. The global ocean output files are displayed on a standard regular grid at 1/12° (approximately 9 km) and 50 standard levels. The data used in this article is the daily average sea surface temperature dataset, covering a period of 30 years from 1993 to 2023. The unit is Celsius, the time resolution is day, and the spatial resolution is 1/12°. The specific parameter information of the data is shown in Table 2 (https://data.marine.copernicus.eu/product/).~~

Table 2. Data parameter description

Information	Details
Full Name	Global Ocean Physics Reanalysis
Product ID	GLOBAL_MULTIYEAR_PHY_001_030
Source	Numerical models
Spatial extent	Global Ocean

Spatial resolution	0.083° × 0.083°
Temporal extent	1 Jan 1993 to 31 Dec 2023
Temporal resolution	Daily, Monthly
Elevation levels	50
Processing level	Level 4
Variables	Sea water potential temperature (T)
Feature type	Grid
Blue markets	Polar environment monitoring Policy & governance Science & innovation Extremes, hazards & safety Coastal services Natural resources & energy Trade & marine navigation
Projection	WGS 84 (EPSG:4326)
Data assimilation	In-Situ TS Profiles SST
Update frequency	Annually
Format	NetCDF-4
Originating centre	Mercator Ocean International

155 ~~Table 2. Data parameter description~~

~~Information~~	~~Details~~
~~Full Name~~	~~Global Ocean Physics Reanalysis~~
~~Product ID~~	~~GLOBAL_MULTIYEAR_PHY_001_030~~
~~Source~~	~~Numerical models~~
~~Spatial extent~~	~~Global Ocean~~
~~Spatial resolution~~	~~0.083° × 0.083°~~
~~Temporal extent~~	~~1 Jan 1993 to 31 Dec 2023~~
~~Temporal resolution~~	~~Daily, Monthly~~
~~Elevation levels~~	~~50~~
~~Processing level~~	~~Level 4~~
~~Variables~~	~~Cell thickness~~ ~~Sea water potential temperature (T)~~ ~~Sea water potential temperature at sea floor (T)~~

Feature type	Grid
Blue markets	Polar environment monitoring Policy & governance Science & innovation Extremes, hazards & safety Coastal services Natural resources & energy Trade & marine navigation
Projection	WGS 84 (EPSG:4326)
Data assimilation	In-Situ TS Profiles SST
Update frequency	Annually
Format	NetCDF-4
Originating centre	Mercator Ocean Internationa

3 Methods

3.1 Gradient calculation method

In this paper, the gradient method is used to process the raw sea surface temperature (SST) data to generate temperature gradient maps. At ocean fronts, the seawater parameters change sharply, and their gradients can effectively describe the degree of this variation. The gradient of the SST is calculated to convert the temperature data at the corresponding latitude and longitude coordinates into gradient data, thereby better characterizing the ocean front. Gradient calculations were performed in the neighbourhoods of each data point, and the expression for the gradient calculation is In this paper, the gradient method is used to identify and extract the front. The principle of the gradient method is that there is a relatively high gradient near the ocean front. The pixel gradient is calculated and the pixel higher than a certain threshold is selected to extract the ocean front. The gradient method is simple in principle and fast in calculation, so it is widely used in the detection of ocean fronts.

There is a sharp saltation of seawater parameters in the ocean front, and the gradient of seawater parameters can describe the severity of the change. Therefore, it is necessary to calculate the SST gradient, so as to convert the temperature data under the corresponding longitude and latitude coordinates into gradient data to better characterize the ocean front. Gradient calculations are performed in 3×3 neighborhoods of each data point. The expression of the Gradient calculation is

$$G = \sqrt{D_x^2 + D^2} \quad (1)$$

$$D_x = \frac{T(i, j+1)T - (i, j-1)}{2\Delta X} \quad (2)$$

$$D_y = \frac{T(i+1,j) - T(i,1-j)}{2\Delta T} \quad (3)$$

$$G = \sqrt{D_x^2 + D_y^2} \quad (1)$$

$$D_x = \frac{T(i, j+1) - T(i, j-1)}{2\Delta x} \quad (2)$$

$$D_y = \frac{T(i+1, j) - T(i, 1-j)}{2\Delta y} \quad (3)$$

Where *G* is the SST gradient; Δx、 Δy is the pixel size in the *x* and *y* directions, respectively. *Dx* and *Dy* are the gradient size in the horizontal and vertical directions, respectively, and i and j are the pixel positions in the image, respectively. ~~Where G is the SST gradient; Δ X、 Δ Y is the pixel size in the X and Y directions, respectively. Dx and Dy are the gradient size in the horizontal and vertical directions, respectively, and i and j are the pixel positions in the image, respectively.~~

3.2 Data labels

For the 30-year sea surface temperature gradient map dataset created using the gradient method, ocean front annotations were generated using the Labelme software. To expand the dataset, satellite remote sensing images from different regions and seasons, capable of displaying ocean fronts, were collected. The Labelme annotation tool (typically the Polygon tool) was used to manually annotate the ocean fronts, aiming to group continuous front areas as a single region. Finally, the annotation results were saved as JSON files. By repeating the above steps, a total of 5,000 ocean front annotation datasets were generated.
~~Labelme software was used to generate the ocean front labels First and foremost, data from remote sensing satellite images that show ocean fronts must be gathered, which are from various regions, times of year, and types of houses. Then Labelme's marking tool (typically the Polygon tool) was used to mark ocean fronts. Lastly, the label data were saved as a JSON file. 5000 ocean front label datasets were produced through repeating the above-menthioned procedures.~~

3.3 Construction of the Mask R-CNN model

Mask R-CNN extends Faster R-CNN by adding a branch parallel to the existing target detection frame to predict the target mask. Mask R-CNN has three outputs: a class label, a bounding-box offset and the target mask. The difference between the target mask and the class-box output is that ~~it needs a~~ more refined extraction of the target's spatial layout is needed. The network architecture diagram of Mask R-CNN is shown in Fig.2. The architecture takes a square 224 × 224 pixel RGB image as input and produces a distribution over the ImageNet object classes, which is composed of five convolutional layers, three pooling layers, two ~~fc~~ FC layers, and finally a classifier layer. The success of this architecture is based on several factors, such as the availability of large data sets, increased~~more~~ computing power, and the availability of GPUs. It also depends on the implementation of additional techniques, such as dropout, data augmentation to prevent overfitting, and rectified linear units to accelerate the training phase.

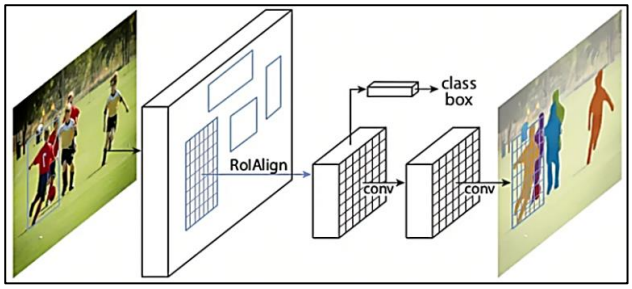

Figure 2. Mask R-CNN network architecture (Gkioxari et al., 2017)

The residual~~Residual~~ neural network (Res-Net) and feature pyramid network (FPN) are the key networks used to extract features in Mask R-CNN. Res-Net is a residual learning framework used to reduce the burden of network training, and the ~~.~~ FPN extracts region of interest (ROI) features from different feature levels~~levels of features~~ according to the size of the features. An RPN (region potential network) region generation network is used to generate candidate regions. Then, ROI Align collects the image features and candidate region features as the input ~~of~~ to the subsequent full connection layer, and then determines the target category.

Applying deep learning methods to ocean front ~~recognition~~detection is challenging~~a challenging task,~~ because fronts have significant visual similarity~~similarities~~ and are indistinguishable i~~o~~n colour and shape. Ocean fronts are regions in which~~where there is a~~ sharp transitions in oceanic properties such as temperature, salinity and density occur. These fronts are critical for understanding the dynamics of the ocean and the global climate system. However, detecting and characterizing these fronts is ~~a~~ challenging ~~task~~ due to their complex and dynamic nature. In particular, the visual similarities among different fronts can make it difficult to distinguish them based on colour and shape alone. Deep learning methods offer a promising approach to overcome these challenges. By leveraging large datasets of oceanographic data, including satellite imagery and in ~~-~~situ measurements, deep learning models can learn to identify the patterns and features that are characteristic of different types of ocean fronts. These models can then be used to classify and characterize fronts with high accuracy and efficiency. To develop effective deep learning models for ocean front ~~recognition~~detection, it is essential to carefully curate and preprocess the training data to ensure that it is representative of the range of oceanographic conditions and front types that may be encountered in the real world. Additionally, the choice of neural network architecture and training parameters ~~have a~~ significantly ~~impact on~~affect the performance of the model, and careful tuning and evaluation are required to ensure optimal results.

In our framework, the ocean front is represented as a pixel band with finite width (i.e., a narrow binary mask region), rather than a single-pixel wide line or a bounding box enclosing a high-gradient region. This approach better reflects the physical nature of the front as a transition zone between two water masses. As a connected region, it is directly compatible with the instance segmentation mask output by Mask R-CNN and the IoU area calculation. While the front is geographically quasilinear, modelling it as a "finite-width band" transforms the problem into a region segmentation task. The task of Mask R-CNN is to predict a corresponding binary mask for each front instance. Then, the IoU is calculated based on the area overlap between the predicted mask and the ground-truth mask, which is used to evaluate the detection performance. This process follows the standard evaluation procedure for instance segmentation. Additionally, we designed a non-maximum suppression (NMS) algorithm based on spatial location and mask similarity specifically for merging duplicate detections of the same front segment in overlapping areas with adjacent tiles and for connecting broken parts across boundaries, thereby forming a complete and continuous front vector.

设置了格式: 字体: 非□ 斜

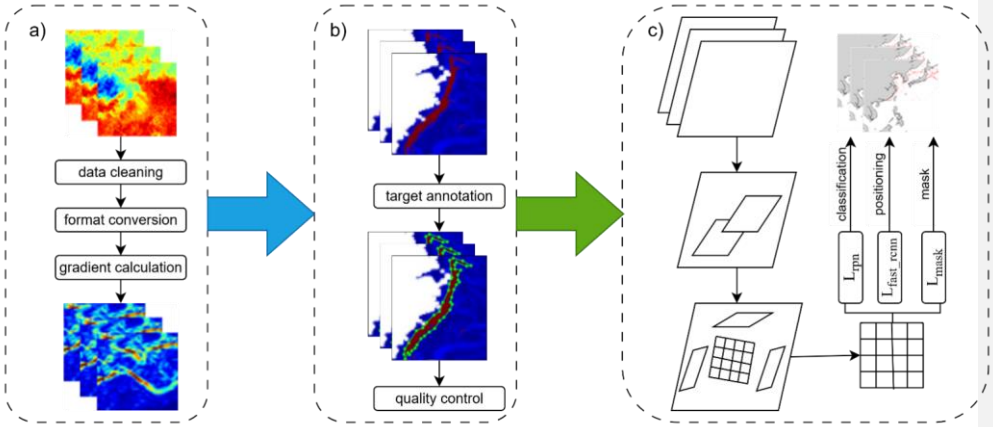

Figure 3. Network architecture diagram for identifying ocean fronts using Mask R-CNN

The ~~loss of~~Mask R-CNN loss involves~~is~~ the addition of the loss on the Mask branch on top of Faster R-CNN~~,~~, which is described as follows~~namely~~:

$$Loss=L_{rpn}+L_{fast\_rcnn}+L_{mask} \quad (4)$$

L_{rpn} generates objects by proposing potential bounding box regions in the image. The L_{fast_rcnn} network extracts the proposed region from the RPN and performs region classification and bounding box regression, and the ~~,~~L_{mask} loss measures the accuracy of the predicted mask by comparing it with the actual mask. By combining these three losses, Mask R-CNN's~~CNN's~~ overall loss function guides the network to simultaneously perform accurate area recommendations, object classification, bounding box regression and instance segmentation. The network learns to balance these different objectives during training to improve its performance in tasks such as object detection and instance segmentation.

The l~~L~~oss function is usually associated with optimization problems, for which it is employed as a learning criterion~~;~~, that is, the model is solved and evaluated ~~to solve and evaluate the model~~ by minimizing the loss function. According to the above task description, the loss function of RPN ~~network~~ training consists of two parts: classification loss and position regression loss.

$$L(\{p_i\},\{t_i\}) = \frac{1}{N_{cls}}\sum_i L_{cls}(p_i,p_i^*) + \lambda\frac{1}{N_{\text{reg}}}\sum_i p_i^* L_{reg}(t_i,t_i^*) \quad (5)$$

$L(\{p_i\},\{t_i\})$ refers to the entire loss function, which represents~~representing~~ the total loss of the model. $\frac{1}{N_{cls}}$ is a scalar that represents~~representing~~ the normalization factor of the classification loss term, where N_{cls} denotes the number of categories in the classification task. $\sum_i L_{cls}(p_i,p_i^*)$ represents the sum of the classification loss terms, which is usually used to measure the performance of the model in classification tasks. The classification loss ~~involving~~ involves each sample i, where p_i is the predicted probability distribution of the model and p_i^* is the probability distribution of the actual label. L_{cls} ~~can~~ is usually ~~be~~ a cross entropy loss or other classification loss function. λ is a non~~-~~negative constant used to balance the classification loss term

and the regression loss term, and $\frac{1}{N_{reg}}$ is the normalization factor for the regression loss term, where N_{reg} represents the number of samples. $\sum_i p_i^* L_{reg}(t_i, t_i^*)$ represents the sum of the regression loss terms. The regression loss for each sample i is involved, where t_i is the predicted regression value of the model and t_i^* is the actual regression target value.

In During the training process, the gradient image of the SST data on the target date was selected to detect and extract the ocean front. Fig.4 provides aAn overview of the experimental workflow is provided in Fig. 4, which illustrates, illustrating the sequential steps involved in detecting and evaluating ocean fronts by using the Mask R-CNN model. This flow chart helps to visualize the process and highlights the key stages in the experiment. The process can be summarized as follows:

1) SST image: The experiment started with by obtaining the SST image data for the study area.

2) Pretreatment: Pre-processing steps for the SST image data were conducted to enhance the quality and remove any noise or artefactartifacts. This step is crucial for ensuringto ensure accurate detection and analysis of ocean fronts.

3) Gradient calculation: The gradient of the SST image was calculated to identify areas of rapid temperature change, which are indicative of ocean fronts. The gradient represents the spatial variation inof temperature across the image.

4) Gradient image: The calculated gradient values were used to generate a gradient image, where higher gradient values correspond to stronger temperature gradients and potential ocean fronts. This image provides a visual representation of the potential ocean front locations.

5) Model training: The Mask R-CNN model was trained by using the gradient image as input. The model learned to identify and classify the ocean fronts based on the patterns and features present in the gradient image. This step involvesd training the model on a large dataset with labelled ocean front samples.

6) Detection results: The trained model was applied to the entire SST image datasetdataset of SST images to detect and localize ocean fronts. The model analyszed each image and identified regions in whichwhere ocean fronts were present.

7) Result eEvaluation of the results: The detection results were evaluated to assess the performance and accuracy of the Mask R-CNN model in terms of detecting ocean fronts. Various metrics, such as the precision, recall, and F1 score, were calculated to measure the model's effectiveness in terms of correctly identifying and locating ocean fronts.

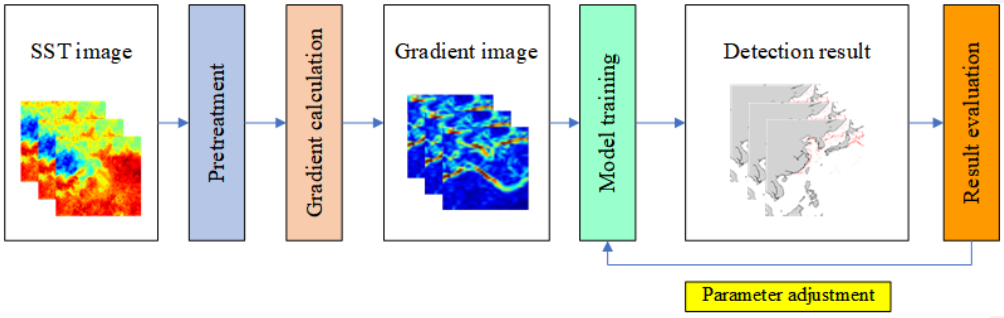

Figure 4. Flow chart of experiment

3.4 Mathematical testing methods

The meanMean average precision (mAP) was chosenused as the evaluation metric. Firstly, the accuracy of the border can bewas represented by the IoU (Intersection over Union), and the general threshold wasis set to 0.5, which means that if the IoU $\geq$ 0.5, the detection is considered correct. Then, by using the recall as the horizontal axis and the accuracy as the vertical axis, the P-R curve can be was obtained. Ideally, both accuracy P and recall R can achieve results that are infinitely close to 1 at the same time. Therefore, it is hoped thatideally, the area covered under the P-R curve is infinitely close to 1. The area below

P-R is called the average accuracy of ocean front detection~~detecting ocean fronts~~, known as the AP (Average Precision). The average of multiple APs is the mAP. The definitions of the IoU, ~~accuracy~~P, ~~recall~~R, and ~~mean accuracy~~AP are as follows:

$$loU = \frac{\text{Area of Overlap}}{\text{Area of Union}} \tag{6}$$

$$\mathrm{P} = \frac{TP}{TP+FP} \tag{7}$$

$$\mathrm{R} = \frac{TP}{TP+FN} \tag{8}$$

$$AP = \int_0^1 \mathrm{P}(\mathrm{R})\,\mathrm{dR} \tag{9}$$

In the equation, the area of overlap~~Area of Overlap~~ refers to the intersection of two prediction boxes, and the area of union~~Area of Union~~ is the union of two prediction boxes. TP denotes the number of ocean fronts recognized by the model as ocean fronts, FP refers to the number of ocean fronts recognized by other objects, and FN refers to the number of ocean fronts recognized as other objects.

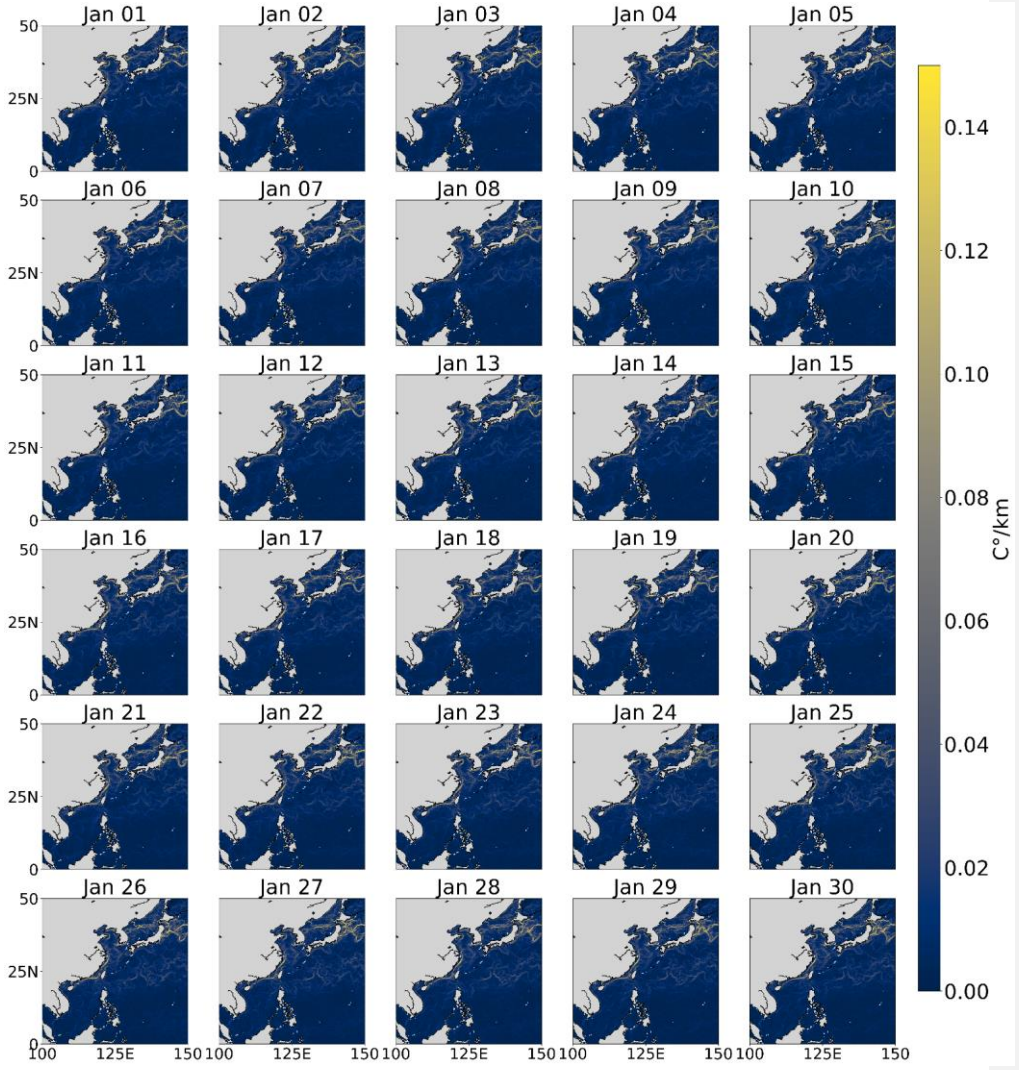

Figure 5. Gradient image of Ocean Front Time Series in January 2023

4 Results and discussion

4.1 Gradient calculation results

To generate the frontal indicator field, we first calculated the temperature gradient by using Formulas (1) – (3). Fig. 5 shows the resulting field for January 2023, which highlights regions in which the sea surface temperature changes rapidly, revealing the spatial structure of the ocean fronts. Warmer colours correspond to stronger transitions. This representation clearly outlines areas of active frontal variability and facilitates a straightforward visual assessment of their distribution and evolution during the month.

~~To create a gradient image, the gradient of the original temperature data was computed using formulas (1) through (3). Fig.5 displays the gradient image of the Ocean Front Time Series in January 2023. The gradient image represents the spatial distribution of ocean fronts, indicating areas of sharp temperature gradients within the specified time period. The colors in the image represent different gradient intensities, with warmer colors indicating stronger gradients. The gradient image provides valuable insights into the spatial patterns and variability of ocean fronts during the specified time frame. It allows for a visual identification of regions with pronounced frontal activity, which is essential for understanding ocean dynamics and processes.~~

4.2 Image marking results

Sufficient training samples are essential for deep learning-based ocean front detection. However, ocean fronts appear as small-scale and weak-edge features in SST imagery, making it difficult to construct a large and effective training dataset, particularly in regions in which the frontal edges are diffuse or ambiguous. To address this limitation, we collected SST images from regions known to exhibit frequent global frontal activity and applied data augmentation and feature enhancement techniques. In addition, a frontal indicator field was derived from the SST data to highlight the frontal structures.

To create the labelled dataset (Fig. 6), each ocean front was manually annotated by using the LabelMe software. Annotators outlined the frontal boundaries in the SST and gradient-enhanced images to generate polygonal masks representing individual fronts. These masks were then converted into COCO-style instance labels to train the Mask R-CNN model.

~~Sufficient training samples are the basis of ocean front detection based on deep learning. As a small scale and weak edge target detection object on SST images, it is difficult to build sufficient and effective training data sets, especially in the weak ocean front area where the edge information of the ocean front is changeable and not obvious. In order to solve this problem, this paper collected SST images of the regions prone to global ocean fronts, and carried out effective expansion and feature enhancement processing. At the same time, the gradient image was obtained by calculating the gradient from the SST data. Then, each ocean front is labeled to form a set of labeled datasets (Fig.6).~~

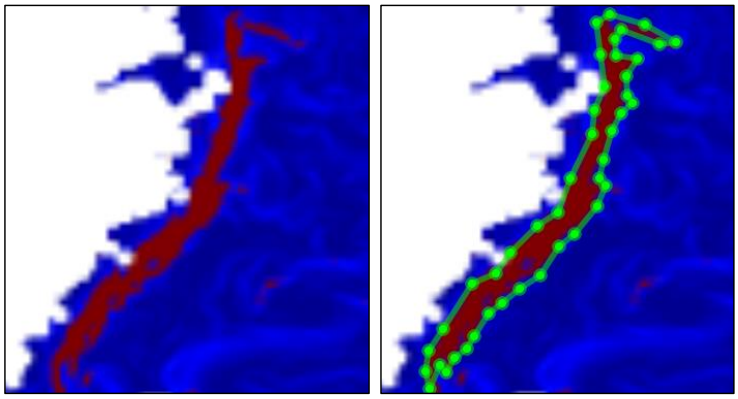

Figure 6. Comparison of the original temperature gradient image and its manual annotation for ocean fronts.

Original temperature gradient image (left panel); manually annotated frontal masks (right panel).

~~Figure 6. The image before marking (left panel) and after marking (right panel).~~

4.3 ~~Recognition~~Detection results of the model

In the field of deep learning, ~~the~~ dataset~~s~~ are divided into three parts: a training set, a validation set, and a testing set. The data in the training set are~~is~~ used to construct~~establish~~ the model, and the~~; The~~ validation set is used to evaluate the predictive performance of each model and choose the model with the best performance; After selecting the model with the best accuracy ~~through~~ via the validation set, the performance of the optimal model is evaluated ~~through~~ on the test set. Notably, to ensure the accuracy of the evaluation,~~It is worth noting that in order to ensure the accuracy of the evaluation~~, the test set data do not need to participate in the training process.~~the test set data needs not participate in the training~~. The quality of the training dataset is the key to affecting the accuracy of the target detection model. To achieve the automatic extraction and learning ~~training~~ of the high-level essential features of ocean fronts in temperature images, a multilevel network model was constructed~~by constructing a multi-level network model~~, thereby achieving the automatic detection and ~~recognition~~detection of ocean fronts. The entire process does not require manual intervention; thus, during~~, so in~~ the dataset construction process, multi-source temperature data were~~is~~ used to ensure the diversity of training data and enhance the generalization ability of the model.

Mask R-CNN ~~has~~ exhibits excellent feature learning ~~ability~~, but it requires multiple adjustments of various network parameters to optimize the network and detection results and thus~~, in order to~~ obtain the best ocean front detection model. The network parameters commonly adjusted in deep learning include ~~Momentum~~the momentum, l~~L~~earning rate, b~~B~~atch s~~S~~ize, w~~W~~eight a~~A~~ttenuation r~~R~~atio, number of iterations, and training test data ratio~~Iteration Times, and Training Test Data Ratio~~. ~~Learning~~ The learning rate is usually set to 0.0002, the weight attenuation is typically set to 0.0005, and the batch size is set to 2 due to memory limitations.~~Weight Attenuation is commonly set to 0.0005, and Batch size is set to 2 due to memory limitations.~~ The network parameter settings with the best detection accuracy are obtained primarily by adjusting the proportion of training test data, the learning rate, and the number of iterations.~~are mainly obtained by adjusting the proportion of training test data, learning rate, and iteration times.~~

In comparative experiments, the proportion of training data gradually decreases while the proportion of test data increases~~;~~, this process aims to evaluate the performance of the model under different data distributions. In our experiments, under the~~which aims to evaluate the performance of the model under different data distributions. Under~~ given learning rates, batch

sizes, and numbers of iterations~~iteration times~~, the average accuracy (AP) and recall (AR) of the model varied with different data ratios, indicating that the proportion of training data has a certain effect on the performance of the model. ~~. This indicates that the proportion of training data has a certain impact on the performance of the model.~~ From the given data, it can be observed that in Experiments 1 and ~~Experiment~~ 2, the average accuracy and recall of the model improved when the training data ratio decreased from 0.8 to 0.75. This outcome may be due to the addition of some test data, which enabled~~s~~ the model to better generalize to unseen data. However, in Eexperiments 3, 4, and 5, as the proportion of training data further decreased, the average accuracy and recall of the model gradually decreased. This finding indicates that the model may not be able to fully learn the features of the data with less training data, leading to performance degradation. In addition, we can also observe that there are certain differences in the average accuracy and recall of the model in different experiments. This phenomenon may be due to changes in the distribution of the data, which resulted~~resulting~~ in the model learning different patterns in different experiments. In summary, the proportion of training data has a certain impact on the performance of the model. In some cases, increasing the proportion of test data can improve the performance of the model, but a low proportion of training data may lead to performance degradation. ~~In order t~~To meet the training and testing requirements, 75% of the samples ~~are~~ were used as the training set for model training, and 25% were used as the test set to evaluate the generalization error of the model after training. By continuously adjusting the model parameters during model training, the optimal parameter combination was~~is~~ selected according to the ocean front detection effect ~~of ocean front~~.

Table 3. Comparison of training model results under different training and testing ratios

serial number	The proportion of training data	The proportion of test data	Learning rate	Batch Size	Number of iterations	AP	AR
1	0.8	0.2	0.0002	2	1000	0.918	0.893
2	0.75	0.25	0.0002	2	1000	0.929	0.907
3	0.7	0.3	0.0002	2	1000	0.921	0.898
4	0.65	0.35	0.0002	2	1000	0.902	0.846
5	0.6	0.4	0.0002	2	1000	0.897	0.812

To verify the accuracy of the model's detection results, the model was tested by using the test dataset, and the mAP was calculated. The results were compared with the manually annotated results, and the IoU value was also computed. Additionally, to further improve the ocean front detection performance, the model parameters were continuously adjusted to enhance both the mAP and IoU. Finally, after 30,000 iterations, the trained network successfully demonstrated the ability to detect ocean fronts. The training loss and detection mAP according to different numbers of iterations are shown in Table 4.

After 30,000 iterations, the training effectively converged and gradually decreased, and the model's detection mAP improved to 0.9. The data in the table indicate that as the number of training iterations increased, the training loss gradually decreased, whereas the detection mAP gradually improved. After 5,000 iterations, the loss was 0.327, the IoU was 0.671, and the mAP was 0.680. As the number of iterations increased, the loss decreased, whereas the mAP improved. After 10,000 iterations, the loss decreased to 0.195, the IoU increased to 0.758, and the mAP improved to 0.770. With continued training, both the loss and mAP continued to improve. After 15,000 iterations, the loss decreased to 0.156, the IoU exceeded 0.8, and the mAP reached 0.830, and after 20,000 iterations, the loss further decreased to 0.133, and the mAP increased to 0.860. After 25,000 iterations, the loss decreased to 0.127, and the mAP reached 0.880. Finally, after 30,000 iterations, the loss decreased to 0.118, the IoU increased to 0.916, and the mAP reached 0.920.~~In order to verify the accuracy of the model detection results, the model is tested with the test data set, the mean average precision (mAP) of the model is calculated, and the results are compared with the manual labeling results, and the intersection overlap (IoU) value is calculated. In addition, in order to further improve the detection results of the ocean front, the model parameters are constantly revised to improve the mAP and IoU. After 30000~~

~~iterations, the training network has the ability to detect ocean fronts. The training loss and recognition accuracy (mAP) of the network with different iterations are shown in Table 4. It can be seen that after 30000 iterations, the training has effectively converged and gradually decreased, and the detection accuracy of the model has also increased to 0.9. According to the provided table data, it can be observed that the training loss and recognition accuracy (mAP) of the network improve with the increase of training iterations. At the beginning, as the training progressed to 5000 iterations, the loss was 0.327 and the recognition accuracy was 0.680. As the number of iterations increases, the loss gradually decreases, while the recognition accuracy gradually increases. At 10000 iterations, the loss decreased to 0.195 and the recognition accuracy improved to 0.770. As the training continues, the loss and recognition accuracy continue to improve. At 15000 iterations, the loss decreased to 0.156 and the recognition accuracy reached 0.830. At 20000 iterations, the loss further decreased to 0.133 and the recognition accuracy improved to 0.860. After 25000 iterations, the loss decreased to 0.127 and the recognition accuracy reached 0.880. Finally, after 30000 iterations, the loss was further reduced to 0.118 and the recognition accuracy reached 0.920. Based on these observations, it can be concluded that as the number of training iterations increases, the training loss of the network gradually decreases, while the recognition accuracy gradually improves.~~

These findings indicate~~This indicates~~ that the network gradually learns better feature representation and classification capabilities during the training process, thereby improving its performance in ~~recognition~~detection tasks. Notably, although both the loss and detection accuracy significantly improved during the training process~~It is worth noting that although both loss and recognition accuracy have significantly improved during the training process~~, the improvement in the loss speed seems to slow down after 30000 iterations, whereas the detection accuracy still further improved~~the improvement speed of loss seems to slow down after 30000 iterations, while recognition accuracy still has further improvement~~. This finding may indicate that the network has approached or reached its optimal performance on this dataset, and further training may ~~only~~ result in only minor improvements. In summary, based on the provided data, ~~it can be seen that~~ the loss and ~~recognition~~detection accuracy of the training network improve with an increasing number of training iterations~~the increase of training iterations~~, indicating that the performance of the network in learning tasks ~~is~~ gradually ~~improving~~improves.

Table 4. Training network loss and ~~recognition~~detection accuracy rate

Iterations	loss	IoU	mAP
5000	0.327	0.671	0.680
10000	0.195	0.758	0.770
15000	0.156	0.820	0.830
20000	0.133	0.864	0.860
25000	0.127	0.871	0.880
30000	0.118	0.916	0.920
35000	0.120	0.897	0.903

Fig. 7 shows~~In Fig. 7,~~ the ~~recognition~~detection results ~~of for~~the ocean fronts based on the Mask R-CNN model in January 2023 ~~are shown~~. Through the application of deep learning algorithms, the positions and shapes of ocean fronts were identified and displayed~~ by~~ using markers and contours. From the graph, it can be observed that the ocean front ~~recognition~~detection results based on deep learning algorithms can display obvious features. Furthermore, the~~The~~ position and shape of the ocean front are clearly visible in the figure, indicating that the algorithm can effectively capture the spatial distribution of the ocean front and accurately distinguish it from the surrounding sea area. Second~~ly~~, the ocean front ~~recognition~~detection results shown in the figure demonstrate~~d~~ the manifestation of small-scale information. Ocean fronts typically have complex shapes and variations, including slender strip structures and local eddies. Deep learning algorithms can capture these small-scale features, making the ~~recognition~~detection results more refined and continuous.

In addition, the ocean front ~~recognition~~detection results based on the Mask R-CNN model show good continuity over a time

range. The ocean front shown in the figure exhibits a relatively stable distribution and evolution trend over time, indicating that the ~~recognition~~detection algorithm has high stability and reliability, and can effectively track and analy~~sz~~e changes in~~the change process of~~ the ocean fronts.

To further test the accuracy of deep learning methods in terms of identifying ocean fronts, ~~the~~ sea surface temperature data for April 2023 ~~was~~ were used, and ocean fronts were extracted by employing the ~~based on~~ traditional gradient method. Fig.8. shows the ~~results of~~ ocean fronts extracted by both the traditional methods and the deep~~depth~~ learning model. Compared with traditional methods,~~It can be seen that~~ the ocean fronts extracted by the deep~~depth~~ learning model haves~~s~~ a higher ~~fitting~~ degree ~~compared with traditional methods~~of fit, and in addition, the deep learning model can better reflect the small-scale characteristics of ocean fronts. More importantly, the deep learning model is more accurate and saves time and effort.

~~, and can better reflect the small-scale characteristics of ocean front. More importantly, the deep learning model is more accurate and saves time and effort to identify the ocean front.~~

设置了格式: 英□ (英国)

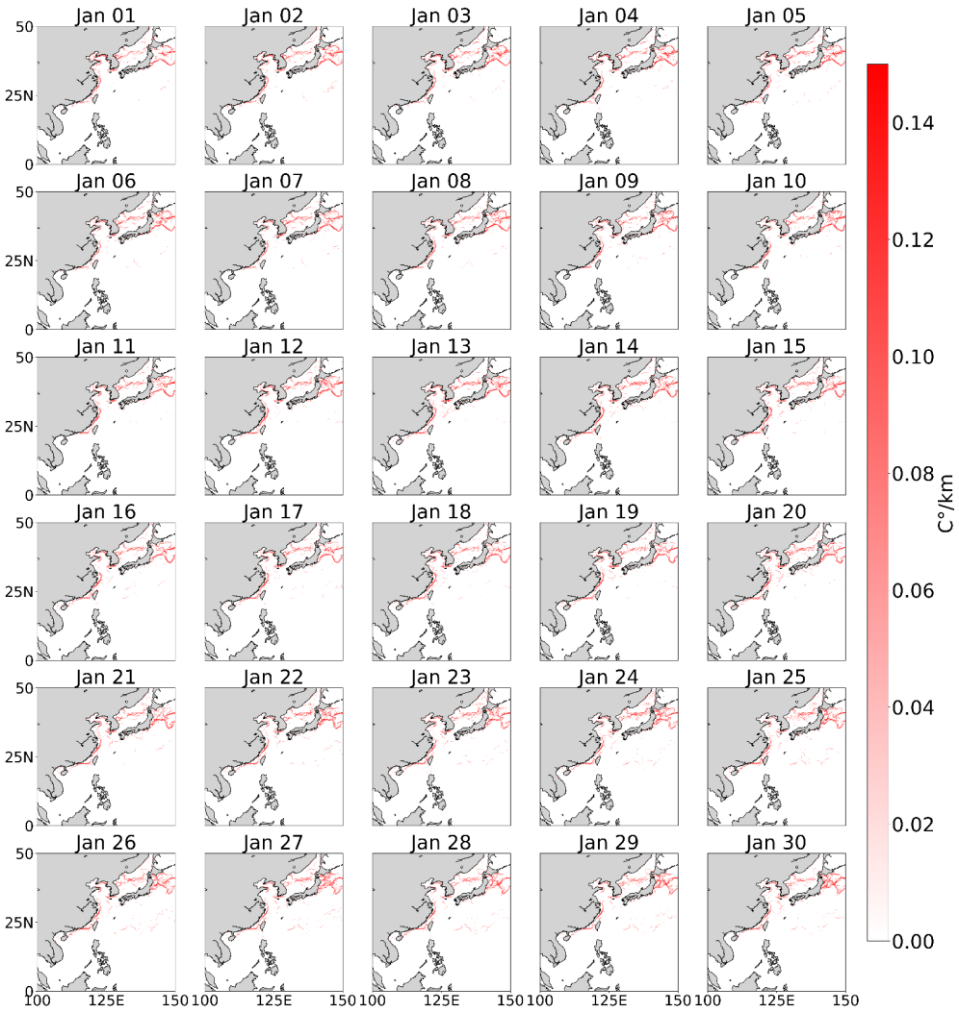

Figure 7. Identification Results of Ocean Front Time Series in January 2023

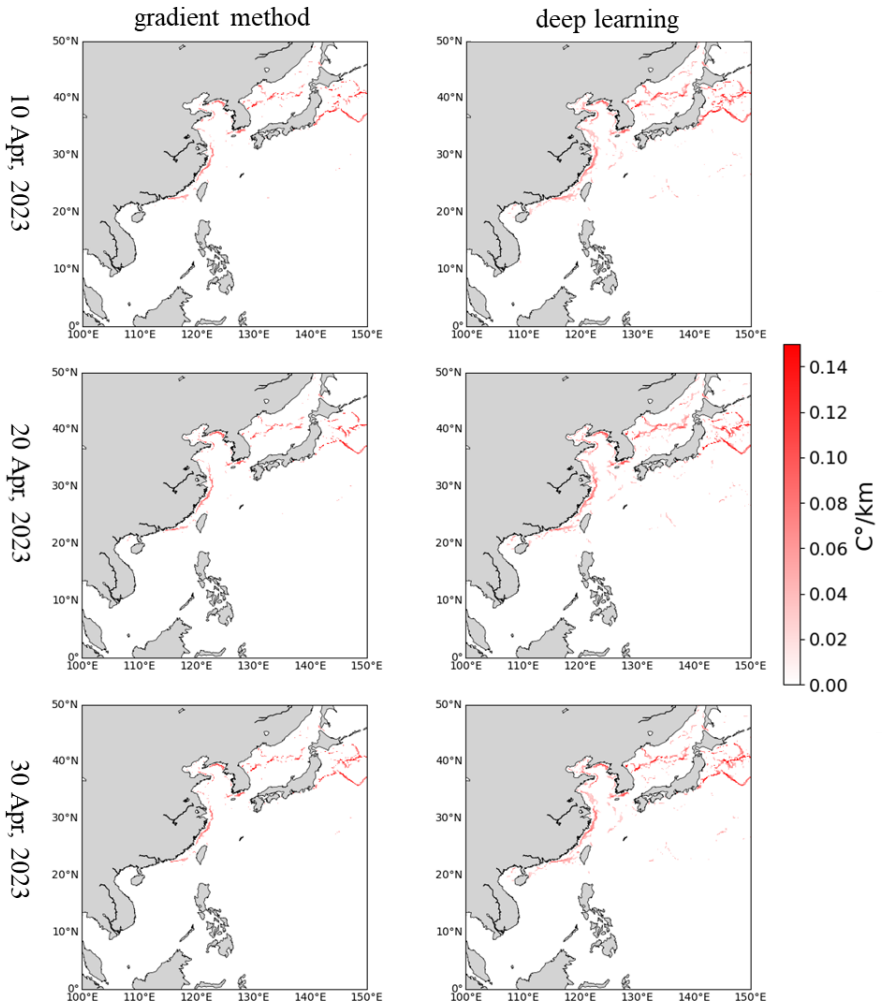

Figure 8. Comparison of Ocean Front Results in April 2023. (Left: Gradient method ~~recognition~~detection results; Right: Deep learning ~~recognition~~detection results)

Furthermore, based on the ocean front detection results, the intensity and width at the corresponding latitude and longitude were extracted, thereby enabling intelligent extraction of the position, intensity, and width of the ocean fronts. Here, intensity refers to the temperature gradient magnitude, and the width was calculated as the distance from the centerline to the boundary. As shown in Fig. 8, the intensity and width of the ocean fronts identified by traditional and deep learning methods were also examined. The numerical results are shown in Table 5. In terms of the intensity of a single ocean front, the table presents both the gradient-based and deep learning–based measurements, which are expressed in degrees °C/km with an error of 0.013 °C/km. The width of a single ocean front detected by the gradient and deep learning methods is measured in kilometres with an error of 0.155 km. These results indicate that the deep learning method is consistent with the gradient detection method in terms of capturing ocean front characteristics. Overall, these findings highlight the effectiveness of the deep learning approach in ocean front detection.

~~Calculate the feature elements of the ocean front, extract the intensity and width of the ocean front at the corresponding longitude and latitude based on the recognition results of the ocean front, and thus achieve intelligent extraction of the position, intensity, and width of the ocean front. According to the comparison results in Figure 8, statistical analysis was conducted on the accuracy indicators of ocean fronts identified by traditional methods and deep learning methods, as shown in Table 5. The Monthly Average Gradient Detection Frontal Quantity indicates the average number of detected ocean fronts using gradient detection methods on a monthly basis. On the other hand, the Monthly Average Number of Deep learning Detection Fronts represents the average number of ocean fronts detected using Deep learning methods. The Detection Quantity Accuracy column shows the accuracy of the detection quantity, which is calculated as the percentage of Deep learning detection fronts compared to gradient detection fronts.~~

~~For the intensity of single ocean front, the table displays the Gradient and the Deep learning Detection of Single Ocean Front Intensity. Both are measured in degrees Celsius per kilometer. The difference between the two methods is shown in the Error (℃/km) column, which represents the absolute difference (error) between the gradient detection and Deep learning detection of single ocean front intensities. The reported error is 0.013 ℃/km. Furthermore, the table provides information about the width of single ocean front. The Gradient and the Deep learning Detection of Single Ocean Front Width are measured in kilometers. The Error (km) column represents the absolute difference (error) between the gradient detection and Deep learning detection of single ocean front widths. In this case, the error is reported as 0.155 km.~~

~~Overall, table V demonstrates the performance and accuracy of the Deep learning method in detecting ocean front characteristics. The high accuracy of the detection quantity suggests that the Deep learning method successfully identifies a significant number of ocean fronts. The small errors in both intensity and width measurements indicate that the Deep learning method closely aligns with the gradient detection method in capturing the characteristics of ocean fronts. These findings highlight the effectiveness of the Deep learning approach for detecting and analyzing ocean fronts.~~

Table 5. Precision Indicators of Ocean Front Characteristics

Statistical indicators	Traditional methods	Deep learning	Error
~~identifying the number of ocean fronts~~	~~11~~	~~13~~	~~2~~
Single Ocean Front Intensity (℃/km)	0.112	0.125	0.013
single ocean front width (km)	27.124	27.279	0.155

4.4 Analysis of seasonal changes and spatio-temporal characteristics

Research on the seasonal patterns of ocean fronts is extremely important for better understanding the Earth's climate system, as it helps to gain a deeper understanding of ocean circulation and its impact on seawater temperature, salinity, and nutrient distribution, which is crucial for ecosystems, fisheries, and marine resource management.

The ocean front detection results for the entire year of 2023 are divided by season: spring (March, April, and May), summer (June, July, and August), autumn (September, October, and November), and winter (December, January, and February). In

addition, the seasonal averages were calculated to obtain the spatial and temporal distributions of ocean fronts during each season. In terms of the seasonal distribution, ocean front activity is most frequent and most common in the winter, followed by the autumn. Spring and summer have relatively fewer ocean fronts, with the lowest number observed in summer. In terms of the number of ocean fronts, the order, from the fewest to the most numerous, is summer < spring < autumn < winter. Regarding spatial distribution, ocean fronts are more active in nearshore waters. In the South China Sea, ocean fronts are concentrated primarily between Hainan and the Taiwan Strait, with a higher frequency of ocean fronts near the Taiwan Strait. In spring and summer, ocean front activity in the South China Sea is relatively inactive, with fewer ocean fronts. In terms of seasonal and spatial distribution characteristics, the results align with prior observations (Hickox et al., 2000).

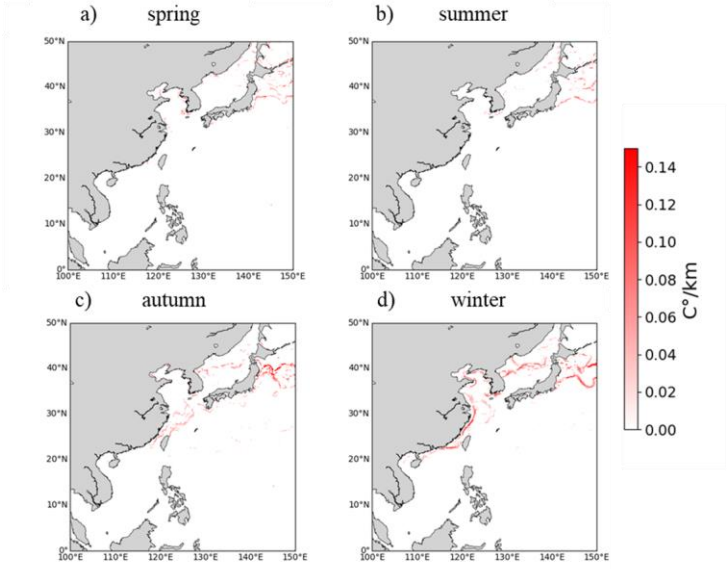

Figure 9. Seasonal spatial-temporal distribution map of ocean fronts in 2023

~~The study on seasonal patterns of ocean fronts is extremely important to better understand the Earth's climate system. It helps to gain a deeper understanding of ocean circulation, its impact on seawater temperature, salinity, and nutrient distribution, which is crucial for ecosystems, fisheries, and marine resource management.~~

~~The recognition results for the entire year of 2023 were divided into spring (March, April, and May), summer (June, July, and August), autumn (September, October, and November), and winter (December, January, and February) and seasonally averaged to obtain the spatio-temporal distribution results of ocean fronts in spring, summer, autumn, and winter.~~

~~From a seasonal distribution perspective, ocean fronts are the most active and numerous in summer, followed by spring. The number of ocean fronts is relatively small in autumn and winter, and the number of ocean fronts is the lowest in winter. In terms of the number of ocean fronts, summer>spring>autumn>winter. From the perspective of spatial distribution, the activity of ocean fronts is relatively frequent in the waters near land. In the South China Sea, ocean fronts are mainly concentrated between Hainan and the Taiwan Strait, and there are many ocean fronts near the Taiwan Strait. In autumn and winter, the activity of ocean fronts in the South China Sea is not active and the number is relatively small.~~

~~Overall, spring and summer are the seasons with more oceanic front activity, especially in coastal areas. The number of fronts in autumn and winter is relatively small and not active.~~

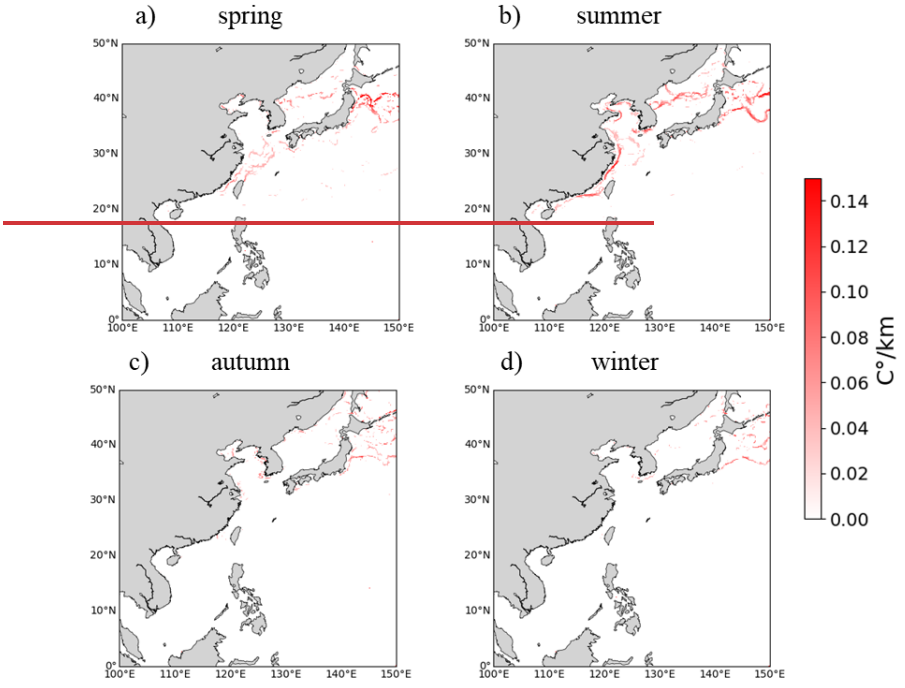

~~Figure 9. Seasonal spatial-temporal distribution map of ocean fronts in 2023~~

4.5 Discussion

4.5.1 Data source errors

The accuracy of ocean front ~~recognition~~detection is influenced by data quality. If the data include noise or missing values or the data source is inconsistent, the model will~~If there is noise, missing values, or inconsistency in the data source, it will cause the model to~~ learn inaccurate features and introduce errors. The reliance on satellite imagery as the primary data source for the proposed method may limit its applicability in certain situations. In such cases, complementary data sources, such as in situ measurements or marine numerical model results, may ~~contribute to~~ enhance the accuracy and robustness of the model.

Furthermore, meteorological ~~Meteorological~~ conditions such as wind, clouds, and precipitation~~precipitation, and atmospheric pressure~~ may affect the clarity and visibility of satellite images. Adverse weather conditions may cause ocean fronts to be blurry or make their recognition in images difficult. ~~may make ocean fronts blurry or difficult to recognize in the image.~~ Waves, storm surges~~surges~~, eddies, and currents also affect the quality of satellite images. These factors may cause

image noise or distortion, making the detection of spikes more difficult. As the~~The~~ performance of deep learning models depends on the available data, more~~. More~~ high-quality data and ground truth data can provide better model training and validation.

4.5.2 Model errors

The model errors mainly stem~~s~~ from four aspects: (1) Insufficient model complexity: The selected deep learning model is not sufficiently complicated~~ enough~~ to capture complex ocean front patterns, which can lead to errors. (2) Overfitting or underfitting: overfitting refers to the model performing well on training data but not well on new data, which may occur because the model is too complex and learns the noise in the training data. Underfitting occurs because the model is too simple to capture the complexity of the data. Thus, unreasonable~~possibly due to the model being too complex and learning about noise in the training data. Underfitting is due to the model being too simple to capture the complexity of the data. Unreasonable~~ learning rate settings can also affect the accuracy of ~~recognition~~detection. (3) Inaccurate labels: If the data labels used for training the model are inaccurate or the labelling~~and the labeling~~ process is not precise enough, the model will learn the wrong patterns. (4) Lack of sufficient training data: If the amount of ocean front data available for training is limited, the model may not be able to fully learn the various features of the front, resulting in errors.

4.5.3 ~~The i~~Impact of the marine environment

Hydrological conditions: Ocean fronts typically occur at boundaries between different water masses, such as cold and warm water currents or salinity gradients. The rapid changes in hydrological conditions may affect the spatial structure~~shape~~ and position of the fronts, and deep~~front. Deep~~ learning models should be able to~~possess the ability to~~ adapt to these variations~~changes~~.

Seasonal and temporal variations: The position and intensity of ocean fronts may vary significantly across~~in~~ different seasons and time periods. Deep learning models need to be able to capture these seasonal differences.

~~Underwater~~Subsurface conditions: Ocean fronts typically exist not only ~~in~~ at the ocean surface~~,~~ but also extend to the ~~underwater~~subsurface. ~~Underwater~~Subsurface conditions, such as temperature, salinity, and water flow, can also affect the front properties. If relevant ~~underwater~~subsurface data are~~is~~ available, incorporating them~~it~~ into model training may help improve the ~~-~~front ~~recognition~~detection accuracy.

In summary, ~~the~~ errors in the ~~recognition~~detection results when applying deep learning to ocean fronts result~~of ocean front deep learning come~~ from the combined~~comprehensive~~ influence of multiple factors, such as the data quality, data label accuracy, data bias, model complexity, overfitting or underfitting, and training data volume. ~~In order t~~To improve the accuracy of ocean front ~~recognition~~detection, it is necessary to address these factors and continuously optimize the model and data. Future research should focus on addressing these challenges~~the challenges mentioned above~~. This process will include~~includes~~ developing strategies to obtain more labelled data, improving the model's robustness to environmental factors, and exploring the potential of integrating different data sources to increase~~enhance~~ the accuracy and applicability of the method.

5 Data availability

The 30-year ocean front dataset (1993–2023) for the Northwest Pacific is available at https://doi.org/10.5281/zenodo.16921277 (Yuan Niu, 2025).

6 Conclusions

As an important ocean phenomenon, the rapid and accurate detection of ocean fronts is highly important for marine ecology, fishery resources, and typhoon path prediction. Given the scarcity of ocean front data, this study constructed a 30-year

manually labelled ocean front dataset and proposed a deep learning-based method for ocean front detection by using the Mask R-CNN model. The experimental results show that this method can achieve automatic ocean front detection with an accuracy exceeding 90%. To improve the model's detection accuracy, cross-validation techniques were used to optimize the algorithm's hyperparameters, including the learning rate, batch size, and loss function weights, to achieve better performance. Additionally, data augmentation techniques such as rotation, scaling, flipping, and brightness adjustment were applied to enhance the robustness of the model. The use of 30 years of sea surface temperature data provides strong support for a deeper understanding of the seasonal and interannual variations in ocean fronts. By analysing long-term time series data, trends in ocean front changes can be identified, including their seasonal migration and potential climate-driving factors. Overall, the results of this study demonstrate the effectiveness of the proposed method in terms of detecting and extracting ocean fronts and highlight the need for further research and development to fully realize its potential for broad applications in oceanography and climatology.

~~An important ocean phenomenon, rapid and accurate detection of ocean front is of great significance to marine ecology, fishery resources and typhoon path prediction. In view of the scarcity and weak edge characteristics of ocean front data, the data are expanded in various forms to increase the data set effectively. In this study, an ocean front recognition method based on depth learning is proposed, which applies Mask R-CNN model to ocean front recognition research to obtain pixel-level ocean front dataset. The experimental results showed that this method can realize ocean front recognition in an automatic process, and the recognized front has good independence and integrity. Recognition accuracy reaches over 90%. The improved Mask R-CNN model demonstrates superior performance in the detection and extraction of ocean fronts compared to existing methods. The use of deep learning methods has significantly improved the target recognition ability of ocean fronts, enabling more accurate detection of fronts, including small-scale fronts. In order to enhance the accuracy of model recognition, cross validation techniques are used to optimize hyperparameters such as learning rate, batch size, loss function weight, etc. in the algorithm to achieve better performance. More data augmentation techniques were used to increase the robustness of the model such as rotation, scaling, flipping, brightness adjustment, etc. Use of 30 years of long-term sea surface temperature data strongly supports a deeper understanding of the seasonal and interannual variations of ocean fronts. By analyzing long-term series data, it is possible to identify the trend of frontal changes, including their seasonal migration and possible climate driving factors. The deep learning method outperforms traditional methods in extracting feature parameters such as ocean front intensity and width. It is possible to extract the characteristic parameters of ocean fronts more comprehensively, and to deeply explore the properties of ocean fronts, such as their scale, intensity, and evolution, which helps to better understand their reaction to the meteorology and climate. Overall, this study demonstrates the effectiveness of the proposed method in detecting and extracting ocean fronts, while also highlighting the need for further research and development to fully unlock its potential for a wide range of applications in oceanography and climatology.~~

Author contributions. XZ and DZ conceived this study. YN and DZ collected the datasets. YN implemented the research and wrote the original draft of the paper. All the authors discussed the results and revised the manuscript.

Competing interests. The contact author has declared that none of the authors has any competing interests.

Acknowledgements. The authors would like to thank the editors and anonymous reviewers for their valuable comments. The authors thank the Copernicus Marine Environment Monitoring Service (CMEMS) for providing the GLORYS12V1 ocean reanalysis dataset, which is based on the NEMO model and driven by ECMWF ERA-Interim and ERA5 reanalyses.

Financial support. This work was supported in part by the Key Research and Development Program, sponsored by the Ministry of Science and Technology (MOST), under Grant 2023YFC3107701 and Grant 2023YFC3107901; in part by the National Natural Science Foundation of China under Grant 42375143.

References

C. T. A. J. J. o. M. S. Chen, "Chemical and physical fronts in the Bohai, Yellow and East China seas," vol. 78, no. 3, pp. 394-410, 2009.

X. L. Wang, C. L. J. A. M. Wang, and Materials, "Extraction of Ocean Fronts Based on Empirical Mode Decomposition," vol. 701-702, pp. 303-307, 2015.

Z. Lachkar, H. Frenzel, P. Marchesiello, M. Münnich, and G. K. J. N. G. Plattner, "Mesoscale eddy-induced reduction in eastern boundary upwelling systems," vol. 4, no. 11, pp. 787-792, 2011.

M. H. Azevedo, N. Rudorff, and J. A. A. J. R. Sensing, "Evaluation of the ABI/GOES-16 SST Product in the Tropical and Southwestern Atlantic Ocean," vol. 13, no. 2, p. 192, 2021.

V. H. Strass et al., "Mesoscale frontal dynamics: shaping the environment of primary production in the Antarctic Circumpolar Current," 2002.

L. W. O"Neill, D. B. Chelton, and S. K. J. J. o. C. Esbensen, "Observations of SST-Induced Perturbations of the Wind Stress Field over the Southern Ocean on Seasonal Timescales," vol. 16, no. 14, pp. 2340-2354, 2003.

X. Yu, A. C. Naveiragarabato, A. P. Martin, D. G. Evans, and Z. J. G. R. L. Su, "Wind-Forced Symmetric Instability at a Transient Mid-Ocean Front," vol. 46, 2019.

I. M. Belkin, P. C. Cornillon, and K. J. P. i. O. Sherman, "Fronts in Large Marine Ecosystems," vol. 81, no. 1-4, pp. 223-236, 2009.

T. J. R. S. Chronis, "Evaluating the Detection of Mesoscale Outflow Boundaries Using Scatterometer Winds at Different Spatial Resolutions," vol. 13, 2021.

G. S. Saldías, W. J. Hernandez, C. Lara, R. Muoz, and L. J. R. S. Soto-Mardones, "Seasonal Variability of SST Fronts in the Inner Sea of Chiloé and Its Adjacent Coastal Ocean, Northern Patagonia," 2021.

S. Ruiz, MarionaPascual, AnandaOlita, AntonioTroupin, CharlesCapet, ArthurTovar-Sanchez, AntonioAllen, JohnPoulain, Pierre-MarieTintore, JoaquinMahadevan, Amala %J Journal of Geophysical Research, C. Oceans: JGR, "Effects of Oceanic Mesoscale and Submesoscale Frontal Processes on the Vertical Transport of Phytoplankton," vol. 124, no. 8, 2019.

I. M. Belkin and J. E. J. J. o. M. S. O"Reilly, "An algorithm for oceanic front detection in chlorophyll and SST satellite imagery," vol. 78, no. 3, pp. 319-326, 2009.

K. Nieto, H. Demarcq, and S. J. R. S. o. E. Mcclatchie, "Mesoscale frontal structures in the Canary Upwelling System: New front and filament detection algorithms applied to spatial and temporal patterns," vol. 123, no. none, pp. 339-346, 2012.

A. G. P. Shaw and R. J. R. S. o. E. Vennell, "Measurements of an Oceanic Front Using a Front-Following Algorithm for AVHRR SST Imagery," vol. 75, no. 1, pp. 47-62, 2001.

I. M. Belkin and P. J. P. O. Cornillon, "SST fronts of the Pacific coastal and marginal seas," 2003.

L. C. Breaker, T. P. Mavor, and W. W. J. C. S. G. C. P. Broenkow, "Mapping and Monitoring Large-Scale Ocean Fronts Off the California Coast Using Imagery from the GOES-10 Geostationary Satellite," 2005.

A. G. Kostianoy, A. I. Ginzburg, M. Frankignoulle, and B. J. J. o. M. S. Delille, "Fronts in the Southern Indian Ocean as inferred from satellite sea surface temperature data," vol. 45, no. 1-2, pp. 55-73, 2004.

B. Ping, F. Su, Y. Meng, S. Fang, and Y. J. A. O. S. Du, "A model of sea surface temperature front detection based on a threshold interval," 2014.

P. Rameshkumar, R. M. S. J. I. J. o. C. T. Parvathi, and Applications, "Edge Detection Algorithm for Color Images using Logical Operation," vol. 03, no. 02, 2012.

R. P. A, H. D. A, and A. E. N. J. R. S. o. E. B, "Detection of mesoscale thermal fronts from 4km data using smoothing techniques: Gradient-based fronts classification and basin scale application," vol. 164, pp. 225-237, 2015.

J. H. Park and O. Il-Seok, "Wavelet-Based Feature Extraction from Character Images," in International Conference on Intelligent Data Engineering and, 2003.

S. M. Lea and M. J. R. S. o. E. Lybanon, "Finding mesoscale ocean structures with mathematical morphology," vol. 44, no. 1, pp. 25-33, 1993.

X. Cun-Jin, S. U. Fen-Zhen, Z. Jun-Qi, G. Yan-You, and Z. J. M. S. Tian-Yu, "Extracting feature of ocean front based on mathematical morphology," 2008.

P. I. Qingling and H. U. J. S. C. Jianyu, "Analysis of sea surface temperature fronts in the Taiwan Strait and its adjacent area using an advanced edge detection method," no. 07, pp. 79-87, 2010.

T. Shimada, F. Sakaida, H. Kawamura, and T. J. R. S. o. E. Okumura, "Application of an edge detection method to satellite images for distinguishing sea surface temperature fronts near the Japanese coast," vol. 98, no. 1, pp. 21-34, 2005.

S. Gen-Yun, G. Min, W. Xiao-Long, and L. I. J. R. S. I. Sheng-Xue, "Application of Edge Detection to the Sea Surface Temperture Fronts of China East Coast," 2012.

G. Sun, Q. Liu, Q. Liu, C. Ji, and X. J. P. R. Li, "A novel approach for edge detection based on the theory of universal gravity," vol. 40, no. 10, pp. 2766-2775, 2007.

J. J. Oram, J. C. Mcwilliams, and K. D. J. R. S. o. E. Stolzenbach, "Gradient-based edge detection and feature classification of sea-surface images of the Southern California Bight," vol. 112, no. 5, pp. 2397-2415, 2008.

L. Chuan-Yu and W. J. M. S. Fan, "Distributions and intra-seasonal evolutions of the sea surface thermal fronts in the Yellow Sea warm current origin area," 2009.

Fan, WangChuanyu, L. J. C. J. o. Oceanology, and Limnology, "An N-shape thermal front in the western South Yellow Sea in winter," 2009.

C. Yang, F. Rongshuang, B. Muhammad, Y. Xiucheng, W. Jingxue, and L. J. I. J. o. G. I. Wei, "Multilevel Cloud Detection for High-Resolution Remote Sensing Imagery Using Multiple Convolutional Neural Networks," vol. 7, no. 5, p. 181, 2018.

Y. Chen, L. Tang, Z. Kan, M. Bilal, and Q. J. J. o. H. Li, "A novel water body extraction neural network (WBE-NN) for optical high-resolution multispectral imagery," p. 125092, 2020.

Markus et al., "Deep learning and process understanding for data-driven Earth system science," 2019.

K. He, G. Gkioxari, P. Dollar, and R. Girshick, "Mask R-CNN," in International Conference on Computer Vision, 2017.

E. Lima, X. Sun, and Y. Yang, "Application of deep convolutional neural networks for ocean front recognition," Journal of Applied Remote Sensing, vol. 11(4), p. 1, 2017.
Sun et al., "A Multiscale Deep Framework for Ocean Fronts Detection and Fine-Grained Location," 2019.
Q. Li, G. Zhong, and C. Xie, "Weak Edge Identification Nets for Ocean Front Detection," 2019.
C. Xie, H. Guo, and J. Dong, "LSENet: Location and Seasonality Enhanced Network for Multi-Class Ocean Front Detection," ed, 2021.
Q. Li, Z. Fan, and G. Zhong, "BEDNet: Bi-directional Edge Detection Network for Ocean Front Detection," 2020.
Y. Li, J. Liang, H. Da, L. Chang, H. J. I. g. Li, and r. s. letters, "A Deep Learning Method for Ocean Front Extraction in Remote Sensing Imagery," no. 19 , p. 19, 2022.
R. Niu et al., "SQNet: Simple and Fast Model for Ocean Front Identification," vol. 15, no. 9, p. 2339, 2023.
V. Felt, S. Kacker, J. Kusters, J. Pendergrast, K. J. I. T. o. G. Cahoy, and R. Sensing, "Fast Ocean Front Detection Using Deep Learning Edge Detection Models," 2023.
K. Nogueira, O. A. B. Penatti, and J. A. D. J. P. R. Santos, "Towards Better Exploiting Convolutional Neural Networks for Remote Sensing Scene Classification," vol. 61, pp. 539-556, 2016.
G. Gkioxari, K. He, P. Dollár, and R. Girshick, "Mask R-CNN," ed, 2017.
Y. Niu, The 30-year ocean front dataset (1993-2023) for the Northwest Pacific. Zenodo. https://doi.org/10.5281/zenodo.16921277, 2025.

Azevedo, M. H., Rudorff, N., and Aravéquia, J. A.: Evaluation of the ABI/GOES-16 SST Product in the Tropical and Southwestern Atlantic Ocean, Remote Sensing, 13, 192, 2021.
Belkin, I. M. and O'Reilly, J. E.: An algorithm for oceanic front detection in chlorophyll and SST satellite imagery, Journal of Marine Systems, 78, 319-326, 10.1016/j.jmarsys.2008.11.018, 2009.
Belkin, I. M., Cornillon, P. C., and Sherman, K.: Fronts in Large Marine Ecosystems, Progress in Oceanography, 81, 223-236, 2009.
Cayula, J. F. and Cornillon, P.: Edge detection algorithm for SST images, J Journal of atmospheric oceanic technology, 9, 67-80, 1992.
Chen, C. T. A.: Chemical and physical fronts in the Bohai, Yellow and East China seas, Journal of Marine Systems, 78, 394-410, 2009.
Chen, Y., Tang, L., Kan, Z., Bilal, M., and Li, Q.: A novel water body extraction neural network (WBE-NN) for optical high-resolution multispectral imagery, Journal of Hydrology, 125092, 2020.
Chronis, T.: Evaluating the Detection of Mesoscale Outflow Boundaries Using Scatterometer Winds at Different Spatial Resolutions, Remote Sensing, 13, 2021.
Davis, L. S.: A survey of edge detection techniques, 4, 248-270, 1975.
Diehl, S. F., Budd, J. W., Ullman, D., and Cayula, J.-F.: Geographic window sizes applied to remote sensing sea surface temperature front detection, J Journal of Atmospheric Oceanic Technology, 19, 1105-1113, 2002.
Fan, WangChuanyu, and Liu: An N-shape thermal front in the western South Yellow Sea in winter, Chinese Journal of Oceanology Limnology, 2009.
Felt, V., Kacker, S., Kusters, J., Pendergrast, J., and Cahoy, K.: Fast Ocean Front Detection Using Deep Learning Edge Detection Models, IEEE Transactions on Geoscience Remote Sensing, 2023.
Gkioxari, G., He, K., Dollár, P., and Girshick, R.: Mask R-CNN, 2017.
He, K., Gkioxari, G., Dollar, P., and Girshick, R.: Mask R-CNN, International Conference on Computer Vision,
Hickox, R., Belkin, I., Cornillon, P., and Shan, Z. J. G. R. L.: Climatology and seasonal variability of ocean fronts in the East China, Yellow and Bohai Seas from satellite SST data, J Geophysical Research Letters, 27, 2945-2948, 2000.

Lachkar, Z., Frenzel, H., Marchesiello, P., Münnich, M., and Plattner, G. K.: Mesoscale eddy-induced reduction in eastern boundary upwelling systems, Nature Geoscience, 4, 787-792, 2011.
Li, Q., Fan, Z., and Zhong, G.: BEDNet: Bi-directional Edge Detection Network for Ocean Front Detection,
Li, Y., Liang, J., Da, H., Chang, L., and Li, H.: A Deep Learning Method for Ocean Front Extraction in Remote Sensing Imagery, IEEE geoscience remote sensing letters, 19, 2022.
Markus, Reichstein, Gustau, Camps-Valls, Bjorn, Stevens, Martin, Jung, Joachim, and Denzler: Deep learning and process understanding for data-driven Earth system science, Nature, 2019.
Nieto, K., Demarcq, H., and McClatchie, S.: Mesoscale frontal structures in the Canary Upwelling System: New front and filament detection algorithms applied to spatial and temporal patterns, J Remote Sensing of Environment, 123, 339-346, 2012.
Niu, R., Tan, Y., Ye, F., Gong, F., Huang, H., Zhu, Q., and Hao, Z.: SQNet: Simple and Fast Model for Ocean Front Identification, Remote Sensing, 15, 2339, 2023.
Nogueira, K., Penatti, O. A. B., and Santos, J. A. D.: Towards Better Exploiting Convolutional Neural Networks for Remote Sensing Scene Classification, Pattern Recognition, 61, 539-556, 2016.
Oram, J. J., McWilliams, J. C., and Stolzenbach, K. D. J. R. S. o. E.: Gradient-based edge detection and feature classification of sea-surface images of the Southern California Bight, 112, 2397-2415, 2008.
Ping, B., Su, F., Meng, Y., Fang, S., and Du, Y. J. A. O. S.: A model of sea surface temperature front detection based on a threshold interval, 2014.
Roa-Pascuali, L., Demarcq, H., and Nieblas, A.-E.: Detection of mesoscale thermal fronts from 4 km data using smoothing techniques: Gradient-based fronts classification and basin scale application, J Remote Sensing of Environment, 164, 225-237, 2015.
Ruiz, S., MarionaPascual, AnandaOlita, AntonioTroupin, CharlesCapet, ArthurTovar-Sanchez, AntonioAllen, JohnPoulain, Pierre-MarieTintore, JoaquinMahadevan, Amala Effects of Oceanic Mesoscale and Submesoscale Frontal Processes on the Vertical Transport of Phytoplankton, Journal of Geophysical Research, C. Oceans: JGR, 124, 2019.
Saldías, G. S., Hernandez, W. J., Lara, C., Muoz, R., and Soto-Mardones, L.: Seasonal Variability of SST Fronts in the Inner Sea of Chiloé and Its Adjacent Coastal Ocean, Northern Patagonia, Remote Sensing, 2021.
Shaw, A. G. P. and Vennell, R.: Measurements of an Oceanic Front Using a Front-Following Algorithm for AVHRR SST Imagery, Remote Sensing of Environment, 75, 47-62, 2001.
Wang, X. L. and Wang, C. L.: Extraction of Ocean Fronts Based on Empirical Mode Decomposition, Applied Mechanics Materials, 701-702, 303-307, 2015.
Yang, C., Rongshuang, F., Muhammad, B., Xiucheng, Y., Jingxue, W., and Wei, L.: Multilevel Cloud Detection for High-Resolution Remote Sensing Imagery Using Multiple Convolutional Neural Networks, International Journal of Geo-Information, 7, 181, 2018.